Otology & Neurotology
26:767–772 © 2005, Otology & Neurotology, Inc.

Neuro-Otologic Findings in Unilateral Isolated Narrow Internal Auditory Meatus

Ken Ito, Sayaka Suzuki, Toshihisa Murofushi, Shin-ichi Ishimoto, Shinichi Iwasaki, and Shotaro Karino

Department of Otolaryngology, Faculty of Medicine, University of Tokyo, Tokyo, Japan.

Objective: To report neuro-otologic findings concerning the four nerves in the internal auditory meatus (IAM) in patients with isolated congenitally narrow IAM and explore the implications regarding ontogeny of the nerves in the IAM.
Design: Retrospective case series study.
Setting: University hospital.
Subjects: Five consecutive patients between 1997 and 2002 with unilateral isolated narrow IAM demonstrated by high-resolution computed tomography whose chief complaint was hearing loss (1 male and 4 females, 4 right sides and 1 left; age range 5–37 years, mean 20 years; IAM diameter at the porus: 26–33% of that on the normal side).
Main Outcome Measures: Functional studies concerning the VIIth cranial nerve and the three branches of the VIIIth cranial nerve.
Results: In all ears, auditory brain stem responses were absent, the speech discrimination score was 0%, and otoacoustic emissions were absent or markedly reduced compared with those on the normal side. Caloric responses were absent in two ears, reduced in two ears, and normal in one ear. Galvanic body sway tests showed no responses in the two ears in which caloric responses were absent. Inferior vestibular nerve function was estimated as normal in all ears on the basis of vestibular evoked myogenic potential recordings. Facial nerve functions were normal in all patients.
Conclusions: In isolated congenital stenosis of IAM, dysfunction of each nerve in the IAM can occur independently. In the ontogeny of the VIIIth cranial nerve, the cochlear and superior vestibular nerves tended to be involved together, whereas the cochlear and inferior vestibular nerves appeared independent of each other. **Key Words:** Narrow internal auditory meatus—Facial nerve—Cochlear nerve—Vestibular nerve—Ontogeny—Neuro-otological findings.
Otol Neurotol **26**:767–772, 2005.

Nonsyndromic congenitally narrow internal auditory meatus (IAM) is rare, especially as an isolated finding without inner, middle, or external ear anomalies (1–5), whereas acquired stenoses of IAM were more frequently reported, such as osteomas, exostoses, and fibrous dysplasias (6–8). Although single case reports have appeared recently, neuro-otologic dysfunctions have not been well elucidated. It is known that cochlear nerve atrophy sometimes causes a problem after cochlear implant surgery.

Because it is not possible to conduct experimental research on human development, congenital anomalies are very important in giving us a clue to understanding the processes that occur in ontogeny. This study is to report neuro-otologic findings of five cases in our institution and to deduce what occurs during ontogeny of the four nerves in the IAM.

Address correspondence and reprint requests to Dr. Ken Ito, Department of Otolaryngology, Faculty of Medicine, University of Tokyo, 7–3–1 Hongo, Bunkyo-ku, Tokyo 113–8655, Japan; E-mail: itoken-tky@umin.ac.jp

SUBJECTS

Study comprised five consecutive patients between 1997 and 2002 with isolated congenitally narrow IAM demonstrated by high-resolution computed tomography (HRCT) whose chief complaint was hearing loss (1 male and 4 females, 4 right sides and 1 left, age range 5–37 years, mean 20 years). All patients had unilateral narrowing of the IAM. No other osseous anomalies of the body and no other developmental problems were found in any patient.

METHODS

Dimensions of IAM

Measurements were obtained after McClay et al. (9). Diameter of IAM at the porus (average of height and width) and length of IAM were measured using HRCT.

Functional Studies

In all patients, the following tests/recordings were performed: pure-tone audiograms, auditory brainstem responses, speech discrimination scores, distortion product otoacoustic emissions (DPOAEs), caloric responses (ice water, recorded by electronystagmograph), vestibular evoked myogenic

responses (VEMPs), facial nerve scores (House-Brackmann grade), and stapedial reflexes (contralateral stimulation on the normal side). Patients without caloric responses on the affected side underwent galvanic body sway tests (GBSTs). The GBST directly stimulates the vestibular nerves and presumably represents the function of the superior vestibular nerve innervating the utricle because this test evaluates the lateral sway of the center of foot pressure (10). In patients without VEMPs, electrically evoked myogenic potentials (galvanic-VEMPs) were also recorded. The galvanic-VEMP test, a counterpart of the GBST, also stimulates the vestibular nerves directly and presumably represents the function of the inferior vestibular nerve innervating the saccule because it records the muscular responses similar to the VEMPs of the saccular origin (11,12).

None of the patients had any complaint other than hearing loss. In Cases 1 to 4, profound hearing loss appeared to have been fixed from birth. Case 5 reported episodes that suggested progression of hearing loss. No patients experienced tinnitus or vertigo. On examination, all patients had normal ear drum with type A tympanograms, and none of the patients had nystagmus. A detailed description of Case 1 was published elsewhere (13). Case 5, whose course of hearing loss appeared somewhat atypical compared with the other four cases, is presented below.

CASE PRESENTATION (CASE 5)

A 17-year-old woman was referred to the University Hospital complaining of hearing loss on the right side. When she was 3 years old, she underwent paracentesis for otitis media with effusion. Although right-sided hearing impairment had already been pointed out at that time, there was no further examination. At the age of 15, she noticed right ear fullness and exacerbation of hearing loss. One year later, ear fullness on the right recurred, and she consulted a primary physician. Although she underwent steroid administration therapy under a diagnosis of sudden deafness, there was no improvement in hearing. She did not experience tinnitus, vertigo, or fluctuation of hearing level. Except for hearing impairment, her past history was unremarkable. No one in her family had suffered hearing impairment. Physical examination findings in the head and neck were normal, including the tympanic membranes.

Imaging Study

HRCT

There were no abnormalities found in the external auditory meatus or the middle ear on either side (Fig. 1). The IAM, cochlea, vestibule, and semicircular canals were normal on the left side. Although the inner ear structures were also normal on the right, the right IAM was very narrow, and at the periphery, branched small canals for the four nerves in the IAM were identified.

Magnetic Resonance Imaging

On the left side, inner ear structures were normal, and the cochlear and superior vestibular nerves in the IAM were clearly identified (Fig. 2). On the right side, the cochlea, the vestibule, and the semicircular canals were normal. However, the right cochlear nerve was not identified, whereas the right superior vestibular nerve was clearly visible.

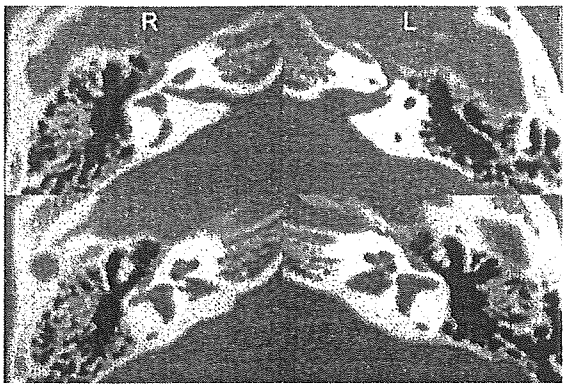

FIG. 1. Axial high-resolution CT scans of the internal auditory meatus (IAM). Compared with the normal left IAM (L), the right IAM (R) is much narrower, and shows branching in the IAM.

Neuro-Otologic Findings

Auditory

Pure-tone audiometry demonstrated sensorineural hearing impairment of the right ear (pure-tone average 73 dB) and normal hearing in the left ear (Fig. 3*A*). DPOAE studies confirmed normal responses in the left ear but very poor responses in the right ear, indicating severe impairment of the outer hair cell (OHC) function (Fig. 3*B*). Auditory brainstem response showed a normal response in the left ear but no response in the right ear.

Vestibular

The patient did not demonstrate nystagmus, dysequilibrium, or ataxia. Caloric responses were normal on the left but absent on the right side. GBSTs showed normal responses (deviation of 11 mm) on the left, but there were no responses on the right side. VEMPs (click) were normally recorded on the left but were absent on the

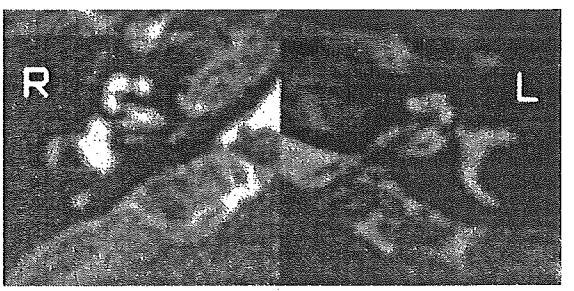

FIG. 2. Axial three–dimensional-constructive interference on steady state (3d-CISS) MRIs. On the left side, cochlear and superior vestibular nerves are identified in the fluid (high) intensity in the IAM. However, on the right, only the superior vestibular nerve can be identified, and the narrow route to the cochlea, seen in the CT, is filled with the fluid intensity.

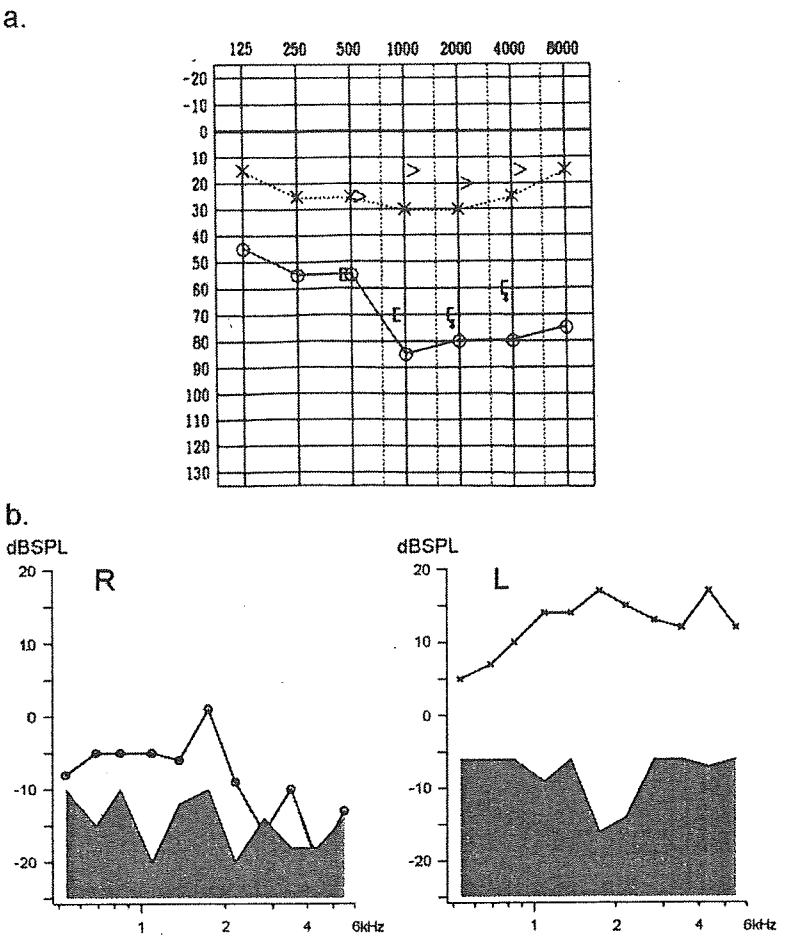

FIG. 3. (*A*) Audiograms. (*B*) DPOAEs.

right side (Fig. 4*A*). However, galvanic VEMPs (3 mA, 1 ms) were normally recorded on both sides (Fig. 4*B*).

Other

Type A tympanograms were recorded on both sides. SRs were normally recorded on the right ear when the tones were delivered to the left ear, indicating normal facial nerve function on the right side. Physical examinations of facial nerve functions were normal. Other cranial nerve tests demonstrated the absence of abnormalities.

RESULTS

Dimensions of IAM

The diameter of the IAM on the affected side was 1.4 to 2.2 mm, mean 1.8 mm (26–33% of that on the normal side), and the length was 12 to 17 mm, mean 14 mm (93–109% of that on the normal side).

Functional Studies

The test results are summarized in Table 1. Pure-tone average was immeasurably high, and no DPOAE responses were found in four patients (Cases 1–4). One patient (Case 5) had severe sensorineural hearing loss with markedly reduced DPAOE responses compared with the normal side. In all ears, auditory brain stem responses were absent, and the speech discrimination score was 0%. Caloric responses were absent in two ears, reduced in two ears (canal paresis 30–40%), and normal in one ear. GBSTs did not show any responses in the two ears in which caloric responses were absent, whereas the normal sides showed normal responses. VEMPs were normally recorded in four ears. In one patient (Case 5) in whom VEMPs were absent on the affected side, galvanic-VEMPs were normally recorded on the same side, suggesting that inferior vestibular nerve function was normal and that the lesion existed in the inner ear (i.e., saccule). Facial nerve functions were normal in all patients.

DISCUSSION

Table 2 shows functional findings in each of the four partitions in the IAM (cochlear, superior vestibular,

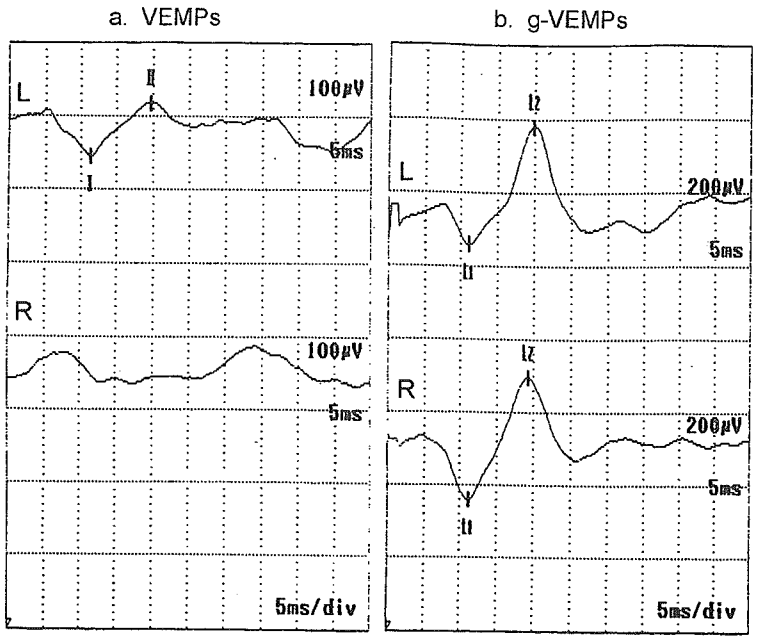

FIG. 4. Recordings of vestibular evoked myogenic potentials (*A*) and galvanic VEMPs (*B*). Stimuli were ipsilaterally delivered as rarefaction clicks of 95 dBn HL for VEMPs (stimulation rate 5 Hz, analysis time 50 ms, averaging 200 traces) and ipsilaterally delivered 3 mA current for 1 ms for g-VEMPs.

inferior vestibular, and facial partitions). In the cochlear partition, OHC damage and impairment of cochlear nerve or inner hair cells can be discriminated by functional tests. In the inferior vestibular partition, nerve damage can be detected by galvanic-VEMPs. However, in the superior vestibular partition, labyrinthine and retrolabyrinthine damage cannot be discriminated at present. GBST is a candidate for detecting superior vestibular nerve damage because body sway is considered to reflect utricular responses. As to the cochlear partition, severe inner ear or cochlear nerve dysfunction was found in all ears. Superior vestibular partition was variably impaired: severe impairment in two ears, moderate impairment in two ears, and normal function in one ear. Inferior vestibular partition was principally not impaired, with one exception (Case 5), in which saccular impairment, but not inferior vestibular nerve dysfunction, was found. The facial nerve was not affected.

Not many articles reported vestibular findings in narrow IAM (1,14–19). OHC function was poor or absent in all four ears in which otoacoustic emission responses were measured, caloric responses were present in three of the seven ears tested, and VEMPs were normally evoked in one ear tested. These reports are in accordance with the present findings.

Our results showed that dysfunction of each nerve in the IAM can occur independently. In the ontogeny of the VIIIth cranial nerve, the cochlear and superior vestibular nerves tend to be involved together, whereas the cochlear and inferior vestibular nerves appear independent of each other. This is in clear contrast with congenital inner ear anomalies, in which cochlea and saccule (pars inferior) tend to be coinvolved, and utricle and semicircular canals (pars superior) tend to be preserved (20). The reason for this discrepancy between the inner ear and the primary sensory nerves in terms of developmental coupling among partitions (cochlear, superior vestibular, and inferior vestibular) is unknown. One possible explanation is the difference of neurotrophic factors involved. It is shown that brain-derived neurotrophic factor is the major survival factor for vestibular ganglion neurons, and neurotrophin-3 for spiral ganglion

TABLE 1. *Results of neuro-otologic tests concerning the VIIth and VIIIth cranial nerves*

Case	Age/sex/side	PTA	SDS	OAE	ABR	CP	GBST	VEMP	g-VEMP	FM, SR
1	31/F/R	> 110 dB	0%	no	no	0%		normal		normal
2	5/F/R	> 110 dB	0%	no	no	30%		normal		normal
3	9/F/L	> 110 dB	0%	no	no	40%		normal		normal
4	37/M/R	> 110 dB	0%	no	no	100%	(−)	normal		normal
5	17/F/R	73 dB	0%	poor	no	100%	(−)	(−)	normal	normal

Dark gray indicates afunction, and light gray dysfunction.

PTA, pure-tone average; SDS, speech discrimination score; OAE, distortion product otoacoustic emission; ABR, auditory brain stem response; CP, canal paresis; GBST, galvanic body sway test; (g-)VEMP, (galvanic) vestibular evoked myogenic potential; FM, facial movement; SR, stapedial reflex.

TABLE 2. *Functional findings of each partition of the four nerves in the internal auditory meatus*

Case	Cochlear partition		Superior vest. partition	Inf. vest. partition		
	OHC	IHC and/or nerve	LSCC and/or nerve	Saccule	Nerve	Facial nerve
1	(++)	(++)	(−)	(−)	(−)	(−)
2	(++)	(++)	(+)	(−)	(−)	(−)
3	(++)	(++)	(+)	(−)	(−)	(−)
4	(++)	(++)	(++)[a]	(−)	(−)	(−)
5	(+)	(++)	(++)[a]	(++)	(−)	(−)

[a]Superior vestibular nerve dysfunction was confirmed by galvanic body sway test.
Dark gray indicates afunction, and light gray dysfunction.
(++) Afunction or severe dysfunction; (+) Impaired function; (−) Normal function.
OHC, outer hair cell; IHC, inner hair cell; LSCC, lateral semicircular canal.

neurons (21). However, the difference between superior and inferior vestibular ganglion neurons has not yet been elucidated. For example, this coupling between cochlear and superior vestibular partitions could be accounted for if the superior vestibular ganglion neurons also depended partly on neurotrophin-3 as well as on brain-derived neurotrophic factor.

In this study, we used CT to evaluate the abnormality of the IAM because magnetic resonance imaging is of limited use with a narrow IAM in contrast with the cochlear nerve aplasia with a normal-sized IAM in which nerve bundles can be visualized in the high-intensity IAM space with T2-weighted images (22). Although magnetic resonance imaging was useful in a certain, rather exceptional, occasion with a narrow IAM (13), it is usually not possible to discriminate between cochlear nerve aplasia and hypoplasia even with the highest resolution because nerve bundles are not well visualized in the small IAM space with T2-weighted images and because it is difficult to identify a very thin nerve bundle using T1-weighted images.

From the smooth outlines of the narrow bony canals, it is supposed that the narrowing was formed congenitally by the excessive bone proliferation around the atrophic nerves in the course of ontogeny. Acquired stenosis such as fibrous dysplasia or osteoma causes the outlines of the stenotic canal to look irregular, showing constriction only at the portion where the lesion existed (6,7). Neural growth factors excreted from the developing otic capsule induce the VIIIth cranial nerve, and the mesoderm eventually transforms into cartilage and ultimately ossifies around the VIIth and VIIIth cranial nerve, forming the IAM. Therefore, it is assumed that IAMs can normally be formed around normal VIIIth nerves only (1,3). Although the normally shaped cochlea demonstrated by imaging studies suggests that the cochlea was formed during ontogeny, impairment of the organ of Corti in all affected ears of the patients, demonstrated by otoacoustic emission testings that showed OHC dysfunction, supports this hypothesis.

A question remains regarding the onset of hearing loss in Case 5. In addition to the congenital hearing loss caused by the hypoplastic VIIIth nerve, there is a possibility of progression. The cochlea and the hypoplastic cochlear nerve might have been further damaged postnatally for certain reasons (e.g., a sudden decrease in cochlear blood supply caused by inflammation, edema and so on) because the cochlear artery is an end artery. In this relation, acquired facial palsy in a case of IAM stenosis was previously reported (15). Therefore, when this disorder is encountered, we suggest that the thorough neuro-otologic examination, preferably including inferior vestibular nerve evaluation, should be performed and that the patient should be followed up on a regular basis (e.g., once per 1–2 years).

REFERENCES

1. Yates JA, Patel PC, Millman B, et al. Isolated congenital internal auditory canal atresia with normal facial nerve function. *Int J Pediat Otorhinolaryngol* 1997;41:1–8.
2. Casselman JW, Offeciers FE, Govaerts PJ, et al. Aplasia and hypoplasia of the vestibulocochlear nerve: Diagnosis with MR imaging. *Radiology* 1997;202:773–81.
3. Shelton C, Luxford WM, Tonokawa LL, et al. The narrow internal auditory canal in children: A contraindication to cochlear implants. *Otolaryngol Head Neck Surg* 1989;100:227–31.
4. Valvassori GE, Naunton RF, Lindsay JR. Inner ear anomalies: Clinical and histopathologic considerations. *Ann Otol Rhinol Laryngol* 1969;78:929–38.
5. Lapayowker MS, Woloshin HJ, Ronis ML, et al. Temporal bone abnormalities in congenital neurosensory deafness as revealed by plesiosectional tomography. *Am J Roentogenol* 1966;97:125–34.
6. Morrissey DD, Schleuning J. Fibrous dysplasia of the temporal bone: Reversal of sensorineural hearing loss after decompression of the internal auditory canal. *Laryngoscope* 1997;107:1336–40.
7. Clerico DM, Jahn AF, Fontanella S. Osteoma of the internal auditory canal. Case report and literature review. *Ann Otol Rhinol Laryngol* 1994;103:619–23.
8. Roberto M, Ettorre GC, Iurato S. Stenosis of the internal auditory canal. *J Laryngol Otol* 1979;93:1211–6.
9. McClay JE, Tandy R, Grundfast K, et al. Major and minor temporal bone abnormalities in children with and without congenital sensorineural hearing loss. *Arch Otolaryngol Head Neck Surg* 2002;128:664–71.
10. Monobe H, Murofushi T. Vestibular testing by electrical stimulation in patients with unilateral vestibular deafferentation: Galvanic evoked myogenic responses testing versus galvanic body sway testing. *Clin Neurophysiol* 2004;115:807–11.
11. Watson SR, Fagan P, Colebatch JG. Galvanic stimulation evokes short-latency EMG responses in sternocleidomastoid which are abolished by selective vestibular nerve section. *Electroencephalogr Clin Neurophysiol* 1998;109:471–4.

12. Watson SR, Colebatch JG. Vestibulocollic reflexes evoked by short-duration galvanic stimulation in man. *J Physiol* 1998;513(Pt 2):587–97.
13. Ito K, Ishimoto S, Murofushi T. Narrow internal auditory meatus: An idiopathic case confirming the origin and pathway of vestibular evoked myogenic potentials in humans. *Arch Otolaryngol Head Neck Surg* 2001;127:275–8.
14. Acker T, Mathur NN, Savy L, et al. Is there a functioning vestibulocochlear nerve? Cochlear implantation in a child with symmetrical auditory findings but asymmetric imaging. *Int J Pediatr Otorhinolaryngol* 2001;57:171–6.
15. Nakamura K, Koda J, Koike Y. Stenosis of the internal auditory canal with VIIth and VIIIth cranial nerve dysfunctions. *ORL J Otorhinolaryngol Relat Spec* 1999;61:16–8.
16. Ochi K, Kinoshita H, Kenmochi M, et al. Neurotological findings in a patient with narrow internal auditory canal: A case report. *Auris Nasus Larynx* 2003;30(Suppl):S93–6.
17. Cho YS, Na DG, Jung JY, et al. Narrow internal auditory canal syndrome: Parasagittal reconstruction. *J Laryngol Otol* 2000;114:392–4.
18. Vilain J, Pigeolet Y, Casselman JW. Narrow and vacant internal auditory canal. *Acta Otorhinolaryngol Belg* 1999;53:67–71.
19. Thai-Van H, Fraysse B, Berry I, et al. Functional magnetic resonance imaging may avoid misdiagnosis of cochleovestibular nerve aplasia in congenital deafness. *Am J Otol* 2000;21:663–70.
20. Schuknecht HF, Igarashi M, Gacek RR. The pathologic types of cochleo-saccular degeneration. *Acta Otolaryngol* 1965;59:154–67.
21. Ernfors P, Van De Water T, Loring J, et al. Complementary roles of BDNF and NT-3 in vestibular and auditory development. *Neuron* 1995;14:1153–64.
22. Thai-Van H, Fraysse B, DeGuine O, et al. Does cochlear nerve aplasia always occur in the presence of a narrow internal auditory canal? *Ann Otol Rhinol Laryngol* 2001;110:388–92.

ORIGINAL ARTICLE

Correlation Between Microtia and Temporal Bone Malformation Evaluated Using Grading Systems

Shin-ichi Ishimoto, MD; Ken Ito, MD; Tatsuya Yamasoba, MD; Kenji Kondo, MD; Shotaro Karino, MD; Hideki Takegoshi, MD; Kimitaka Kaga, MD

Objective: To evaluate the relationships between temporal bone abnormalities and the severity of microtia in Japanese patients using objective grading systems.

Design: Retrospective case series study conducted between 1992 and 2003.

Setting: Academic, tertiary care, referral medical center.

Patients: One hundred forty-two ears of 109 Japanese patients (85 male and 24 female patients; mean age, 12.8 years [range, 2-36 years]) with microtia.

Main Outcome Measures: The severity of microtia was classified according to Marx classification. Developmental abnormalities of the temporal bone were evaluated by a computed tomographic (CT) scoring system modified after the system used by Jahrsdoerfer and colleagues, using high-resolution CT scans of the temporal bone. Correlations between the scores obtained from these 2 grading systems were evaluated using a nonparametric statistical method.

Results: Male preponderance and incidence of bilateral cases of approximately 30% were observed in our Japanese patients with microtia. There was no significant difference in the severity of microtia between unilateral and bilateral cases. The mean±SEM total points in the CT scoring system (full marks, 10) was 7.9±0.4 for grade I microtia, 6.6±0.6 for grade II, and 6.4±0.3 for grade III; the total points correlated inversely with the microtia grade. Development of the auricle correlated significantly with aeration in the middle ear spaces but not with ossicular development or formation of the oval/round windows. Proportion of acceptable surgical candidates according to the CT scoring system (>5 points) was 79% for grade I microtia, 52% for grade II microtia, and 65% for grade III microtia.

Conclusion: The principle "the better developed the auricle, the better developed middle ear" was confirmed in Japanese patients with microtia; however, even with grade II/III microtia, more than half of the patients were considered suitable for atresia surgery.

Arch Otolaryngol Head Neck Surg. 2005;131:326-329

Author Affiliations:
Department of Otolaryngology, Faculty of Medicine, University of Tokyo, Tokyo, Japan (Drs Ishimoto, Ito, Yamasoba, Kondo, Karino, and Kaga); and Department of Otolaryngology, Saitama Medical Center, Kawagoe, Saitama, Japan (Dr Takegoshi).
Financial Disclosure: None.

THE INCIDENCE OF CONGENital aural atresia ranges from 1 in 10000[1] to 1 in 15000[2] births. Congenital aural atresia is a serious birth malformation in which the auricle, the external auditory canal (EAC), middle ear structures, and the inner ear may fail to develop. The degree of microtia ranges from smaller pinna with a normal shape to almost complete absence of pinna with rudimentary soft tissue. The state of the auricle can be classified into 3 types using the classification described by Marx.[3] The EAC anomaly varies from slightly narrow canal to complete atresia.[4-8] Abnormalities of the middle ear structure include stapes deformity, absence of oval and/or round windows, aberrant course of facial nerve, poor pneumatization of the middle ear space, and fusion of malleus and incus.[4-6,9-13] The incidence of inner ear abnormalities associated with microtia is estimated between 10% and 47%.[14]

Surgery for congenital aural atresia is one of the most challenging and difficult procedures in otology because this condition is often accompanied by various temporal bone anomalies, such as aberrant facial nerve, deformity of ossicles, defect of oval window, and lack of mastoid pneumatization.[4,5,7,8,13,15] Preoperative high-resolution computed tomography (HRCT) is indispensable for the surgical planning because it provides important anatomical information. For determining good surgical candidacy, Jarhsdoerfer et al[8] developed a grading system based on preoperative temporal bone HRCT and appearance of the auricle. This computed tomographic (CT) scoring system consists of 9 parameters related to temporal bone anatomy. The presence of a well-defined stapes scores 2 points, whereas all other parameters are assigned 1 point

Table 1. Distribution of 142 Microtic Ears With External Ear Anomalies According to the Criteria of Marx[3] Classification

Grade	Bilateral			Unilateral			
	Right, No.	Left, No.	Subtotal, No. (%)	Right, No.	Left, No.	Subtotal, No. (%)	Total, No. (%)
I	4	7	11 (17)	10	12	22 (29)	33 (23)
II	6	4	10 (15)	3	8	11 (14)	21 (15)
III	23	22	45 (68)	26	17	43 (57)	88 (62)
Total	**33**	**33**	**66 (100)**	**39**	**37**	**76 (100)**	**142 (100)**

each.[8] A presurgical rating of 8 points or more translates into an 80% chance of restoring hearing to near-normal levels.[8,9] This grading system allows accurate prediction of the surgical outcome, and patients with scores less than 6 are considered unsuitable for surgical correction.

The correlation between microtia grade and severity of middle ear abnormalities has been reported.[10] Better developed auricles have more developed middle ear structures and, therefore, the severity of microtia may be used as an indicator of middle ear development in microtia.[10] However, previous studies only examined white patients, and to our knowledge, no studies have yet examined Asian patients. Moreover, the correlation between individual parameters of the CT scoring and microtia grades has not been evaluated. In the present study, we investigated the relationship between severity of microtia and temporal bone abnormalities in a Japanese population.

METHODS

The subjects included 142 ears of 109 patients with microtia (85 male and 24 female patients; mean age, 12.8 years [range, 2-36 years]), who were seen between August 1992 and October 2003 and underwent HRCT examination of the temporal bone at the University of Tokyo Hospital, Tokyo, Japan. Those who had other anomalies associated with systemic syndromes, such as Treacher Collins and Goldenharr syndromes, were excluded from this study.

The severity of microtia was classified into grades I, II, or III according to the classification used by Marx.[3] In brief, grade I microtia exhibits only mild deformity, with the auricle being slightly smaller than normal, each part of which can be clearly distinguished. In grade II microtia, the size of the auricle is one half to two thirds of the normal size and its structure is only partially retained. In grade III microtia, the auricle is severely malformed and usually exhibits a peanut shape.

The HRCT images of the temporal bone were obtained using the Aquilion Multi CT system (Toshiba, Tokyo, Japan). Continuous slices of 1.0-mm thickness were obtained in both axial and coronal planes at 120 kV (peak) and 160 mA. The anomalies of the temporal bone were graded according to the CT scoring system used by Jahrsdoerfer et al,[8] with slight modification, in which the parameter "appearance of external ear" in the original grading system was replaced with the parameter "external ear canal present." The original grading system used by Jahrsdoerfer and colleagues[8] is useful for selection of candidates for atresia surgery. The relationship between the development of the auricle and the structures of the temporal bone was evaluated in the present study. The replacement of the parameter of the "external ear canal present" was more appropriate for this study because the parameter of "appearance of external ear," which is one of the most important elements, was included in the Marx classification.[3] If the external auditory ear was absent or not more than a small mound of skin and cartilage on the face (ie, grade III according to Marx classification[3]) no point was assigned in the classification used by Jahrsdoerfer and colleagues[8]). No other changes were made to the other parameters including their assigned scores.

Table 2. Sex of 109 Patients With Microtia

Sex	Bilateral	Unilateral		Total
		Right	Left	
Male, No.	28	27	30	85
Female, No.	5	12	7	24
Total	**33**	**39**	**37**	**109**

The distribution of parameters of the CT scoring system was examined in relation to the grade of microtia. We also evaluated the correlation between the CT scoring and Marx classification. For correlational analyses, Spearman nonparametric rank correlation coefficient was calculated for Marx classification and total scores of the CT scoring (full mark, 10 points) and between Marx classification and the following 3 subtotal scores reflecting specific development: (1) subtotal of parameters related to ossicular development (sum of "stapes present," "malleus/incus complex," and "incudostapedial connection"; full mark, 4 points); (2) subtotal of parameters related to windows connected to the cochlea (sum of "oval window open" and "round window"; full mark, 2 points); and (3) subtotal of parameters related to aeration of the middle ear cavity (sum of "middle ear space" and "mastoid pneumatization"; full mark, 2 points).

RESULTS

Table 1 gives the distribution of microtic ears according to the side and severity as classified using the Marx classification.[3] The distribution according to the side and sex is given in **Table 2**. There was no significant difference in the severity of microtia between unilateral and bilateral cases (t test, 2-tailed). Male patients were predominant in our sample. Moreover, there was no significant difference in the severity of microtia between male and female patients. The inner ear anomalies such as agenesis of the cochlea and the enlarged vestibular aqueduct were not found in these patients.

Table 3 demonstrates the distribution of parameters of the CT scoring system in relation to the grade of microtia. Correlations with Marx classification were evalu-

Table 3. Distribution of Each Parameter of the Computed Tomographic Scoring System*

Parameter	Assigned Point	Marx Classification, %		
		I	II	III
Related to ossicles				
Stapes present	2	70	52	59
Malleus/incus complex	1	94	100	88
Incudostapedial connection	1	67	48	48
Related to the window's connection to the cochlea				
Oval window open	1	85	71	76
Round window	1	94	95	85
Related to aeration development of middle ear				
Middle ear space	1	100	90	85
Mastoid pneumatization	1	85	62	63
Facial nerve	1	64	57	60
External ear canal present†	1	58	33	9

*Modified after the system used by Jahrsdoerfer and colleagues[8] in relation to the Marx classification.[3]
†$P<.001$.

Table 4. Correlation Between Total/Subtotal Points and the Marx[3] Classification*

Variable	Points, Full Mark	Marx Classification			*r*	*P* Value
		I	II	III		
Total points	10	7.85	6.62	6.35	−0.251	.003
Subtotal points related to development of ossicles, windows, and aeration						
Ossicles	4	3.00	2.52	2.53	−0.136	.11
Windows	2	1.79	1.67	1.61	−0.119	.16
Aeration	2	1.85	1.52	1.48	−0.189	.03

*Data are given as average points and Spearman rank correlation coefficient (*r*) with *P* values.

ated in total points and 3 subtotal points related to ossicles, windows open to the inner ear, and aeration of middle ear (**Table 4**).

Total points correlated significantly with the microtia grade, indicating that better developed auricles have better developed middle ear spaces that are more suitable for surgery. For comparison between microtia grades, 1-way analysis of variance showed a significant difference between mean values by grades ($P=.02$), and the Sheffe test, a post hoc test suitable for multiple comparison, showed a significant difference between grades I and III ($P=.02$). The differences between the other pairs (grades I and II, $P=.23$; grades II and III, $P=.91$) failed to reach statistical significance.

With regard to the 3 subtotal points, only the sum points of aeration of the middle ear correlated significantly with the microtia grade. One-way analysis of variance for intergrade comparison revealed significant difference only with sum points regarding aeration ($P=.02$) and not with sum points regarding ossicles ($P=.29$) or windows ($P=.34$). In the intergrade comparison for sum points regarding aeration, the Sheffe test showed significant difference only between grades I and III ($P=.03$) but not between the other pairs (grades I and II, $P=.22$; grades II and III, $P=.96$). These results indicate that the difficulty of ossicular reconstructive surgery, which is closely related to the existence of oval/round windows and deformity of ossicles, does not necessarily depend on the microtia grade.

The proportion of candidates suitable for surgery according to the CT scoring system (>5 points) was 79% for grade I microtia, 52% for grade II microtia, and 65% for grade III microtia.

COMMENT

Microtia has been reported to occur predominantly in male individuals (male-female ratio, 2:1). Furthermore, the incidence of bilateral microtia is reported at 10% to 30%, with right ear involvement in 55% to 65% of unilateral cases.[1,6,16,17] The findings of the present study in Japanese individuals were similar to the aforementioned data (male-female ratio, 4:1; incidence of bilateral case, 30%; and incidence of right-sidedness in unilateral cases, 51%). The severity of microtia was not different between unilateral and bilateral cases.

A previous study reported that the average atresia score according to CT grading system correlates with the severity of microtia,[10] in which the average atresia score was 8.5 in grade I microtia, 7.2 in grade II microtia, and 5.9 in grade III microtia. Similarly, in our patients, total points of the CT scoring system correlated inversely with the severity of microtia. These results support the principle

"the better developed the auricle, the better developed middle ear."

To our knowledge, the correlation between microtia grades and CT parameters (subtotals) regarding development of specific components of the middle ear has not been reported previously. Our study indicates that auricular development correlated significantly with the aeration in the middle ear spaces but not with the ossicular development or formation of the oval/round window. The auricle, middle ear epithelium lining the air cells, ossicles, and stapes footplate capping the oval window are thought to arise from neural crest cells of the first branchial arch, endodermal cells of the first branchial arch, neural crest cells of the first and second branchial arches, and mesodermal cells of the otic capsule, respectively.[18,19] Differences in correlation among specific components may reflect differences in their origin during development.

Takegoshi and colleagues[15] performed a similar study on patients with mandibulofacial dysostosis and found a positive correlation between attic formation and microtia severity. The antrum and the mastoid air cells were absent in the patients with mandibulofacial dysostosis. In our study, the mastoid air cells were not necessarily absent. The mastoid pneumatization were 85% in grade I, 62% in grade II, and 63% in grade III in these patients with microtia, except for those with systemic syndromes.

Microtia is usually accompanied by atresia or stenosis of the EAC. Abnormal EACs can be classified into 3 types: almost normal; narrowing of the fibrocartilaginous canal; and narrowing and tortuosity of both the fibrocartilaginous and bony parts of the canal. Surgical reconstruction of the EAC and ossicular chain is much easier when the EAC is present, even when it is very narrow and tortuous, because this acts as a landmark to help the surgeon to reach the tympanic cavity more safely. In addition, the presence of the EAC is very closely related to the formation of the manubrium.[20] The presence of the manubrium helps to reconstruct the tympanic membrane in its original position. These were the reasons why we replaced the parameter of "appearance of the auricle" in the original scoring system used by Jahrsdoerfer and colleagues[8] with "existence of EAC." As is evident from the distribution shown in Table 3, the parameter "existence of EAC" correlated significantly with the microtia grade ($P<.001$), confirming that replacement of the parameter in the overall scoring system would be beneficial in determining the candidacy for atresia surgery.

In conclusion, the principle "the better developed the auricle, the better developed middle ear" was confirmed in Japanese cases of microtia; however, even with grade III microtia, more than half of the patients were acceptable candidates for atresia surgery. Auricular development correlates significantly with aeration in the middle ear spaces.

Submitted for Publication: August 10, 2004; accepted December 22, 2004.
Correspondence: Shin-ichi Ishimoto, MD, Department of Otolaryngology, Faculty of Medicine, University of Tokyo, 7-3-1 Hongo, Bunkyo-ku, Tokyo 113-8655, Japan (shinchan-tky@umin.ac.jp).

REFERENCES

1. Granstrom G, Bergstrom K, Tjellstrom A. The bone-anchored hearing aid and bone-anchored epithesis for congenital ear malformations. *Otolaryngol Head Neck Surg.* 1993;109:46-53.
2. Farrior J. Surgical management of congenital conductive deafness. *South Med J.* 1987;80:450-453.
3. Marx H. Die Missbildungen des Ohres. In: Henke F, Lubarsh O, eds. *Handbuch der Spez Path Anatomie Histologie.* Berlin, Germany: Springer; 1926:620-625.
4. Mayer TE, Brueckmann H, Siegert R, et al. High-resolution CT of the temporal bone in dysplasia of the auricle and external auditory canal. *AJNR Am J Neuroradiol.* 1997;18:53-65.
5. Mehra YN, Dubey SP, Mann SB, Suri S. Correlation between high-resolution computed tomography and surgical findings in congenital aural atresia. *Arch Otolaryngol Head Neck Surg.* 1988;114:137-141.
6. Schuknecht HF. Congenital aural atresia. *Laryngoscope.* 1989;99:908-917.
7. Lambert PR. Congenital aural atresia: stability of surgical results. *Laryngoscope.* 1998;108:1801-1805.
8. Jahrsdoerfer RA, Yeakley JW, Aguilar EA, et al. Grading system for the selection of patients with congenital aural atresia. *Am J Otol.* 1992;13:6-12.
9. Yeakley JW, Jahrsdoerfer RA. CT evaluation of congenital aural atresia: what the radiologist and surgeon need to know. *J Comput Assist Tomogr.* 1996;20:724-731.
10. Kountakis SE, Helidonis E, Jahrsdoerfer RA. Microtia grade as an indicator of middle ear development in aural atresia. *Arch Otolaryngol Head Neck Surg.* 1995;121:885-886.
11. Jahrsdoerfer RA. Clinical aspects of temporal bone anomalies. *AJNR Am J Neuroradiol.* 1992;13:821-825.
12. Calzolari F, Garani G, Sensi A, Martini A. Clinical and radiological evaluation in children with microtia. *Br J Audiol.* 1999;33:303-312.
13. Takegoshi H, Kaga K, Kikuchi S, Ito K. Facial canal anatomy in patients with microtia: evaluation of the temporal bones with thin-section CT. *Radiology.* 2002;225:852-858.
14. Swartz JD, Faerber EN. Congenital malformations of the external and middle ear: high-resolution CT findings of surgical import. *AJR Am J Roentgenol.* 1985;144:501-506.
15. Takegoshi H, Kaga K, Kikuchi S, Ito K. Mandibulofacial dysostosis: CT evaluation of the temporal bones for surgical risk assessment in patients of bilateral aural atresia. *Int J Pediatr Otorhinolaryngol.* 2000;54:33-40.
16. Brent B. Auricular repair with autogenous rib cartilage grafts: two decades of experience with 600 cases. *Plast Reconstr Surg.* 1992;90:355-375.
17. Jafek BW, Nager GT, Strife J, Gayler RW. Congenital aural atresia: an analysis of 311 cases. *Trans Sect Otolaryngol Am Acad Opthamol Otolaryngol.* 1975;80:588-595.
18. Lambert PR, Dodson EE. Congenital malformations of the external auditory canal. *Otolaryngol Clin North Am.* 1996;29:741-760.
19. Tewfik T, Der Kaloustain V. *Congenital Anomalies of the Ear, Nose, and Throat.* New York, NY: Oxford University Press; 1997.
20. Ishimoto S, Ito K, Yamasoba T, et al. Does external auditory canal coordinate development of malleal manubrium in human? *Arch Otolaryngol Head Neck Surg.* 2004;130:913-916.

Friedman et al. criticize the use of Muller's maneuver, questioning its reproducibility and validity as predictive tool.[3] They argue that assessment with Muller's maneuver can identify palatal obstruction preoperatively and that elimination of palatal obstruction will increase the airflow postoperatively. Eliminating palatal obstruction may result in increasing negative pressures with subsequent obstruction at a lower level. We fully agree that Muller's maneuver is not a very valuable test to predict the obstruction site. Remodelling the upper airway does have consequences for its dynamics and airflow patterns, which may result in obstruction at tongue base level rather than at hypopharyngeal level. Changing the architecture of the upper airway might be an additional reason why we cannot predict surgical outcomes preoperatively.

Anatomical staging has a large cost-benefit when compared to sleep endoscopy, but we believe that combining the two tests may help improving surgical outcomes even more, since both policies lead to fewer UPPP failures. In case the outcome of both screening tests is equal, there is little reason for concern. In case of conflicting outcome, however, it remains unclear which of the screening modalities is superior. In this respect, more research is mandatory.

CINDY DEN HERDER, MD
Resident of ENT, St. Lucas Hospital Amsterdam
Amsterdam, Netherlands

BIBLIOGRAPHY

1. den Herder C, van Tinteren H, de Vries N. Sleep endoscopy versus modified Mallampatiscore in sleep apnea and snoring. *Laryngoscope* 2005;115:735–739.
2. Hessel NS, de Vries N. Results of uvulopalatopharyngoplasty after diagnostic workup with polysomnography and sleep endoscopy: a report of 136 snoring patients. *Eur Arch Otorhinolaryngol* 2003;260:91–95.
3. Friedman M, Ibrahim HZ, Bass L. Clinical staging for sleep-disordered breathing. *Otolaryngol Head Neck Surg* 2002; 127:13–21.
4. Senior BA, Rosenthal L, Lumley A, Gerhardstein R, Day R. Efficacy of uvulopalatoplasty in unselected patients with mild obstructive sleep apnea. *Otolaryngol Head Neck Surg* 2000;123:179–182.
5. Hessel NS, de Vries N. Increase of the apnoea-hypopnoea index after uvulopalatopharyngoplasty: analysis of failure. *Clin Otolaryngol Allied Sci* 2004 ;29:682–685.
6. Friedman M, Ibrahim HZ, Vidyasagar R, et al. Z-palatoplasty (ZPP): a technique for patients without tonsils. *Otolaryngol Head Neck Surg.* 2004 ;131:89–100.
7. den Herder C, van Tinteren H, de Vries N. Hyoidthyroidpexia: a surgical treatment for sleep apnea syndrome. *Laryngoscope* 2005;115:740–745.
8. Friedman M, Tanyeri H, La Rosa M, et al. Clinical predictors of obstructive sleep apnea. *Laryngoscope* 1999;109: 1901–1907.

Bent (Head-Down) Posture and Aberrant Common Carotid Arteries of the Neck: Another New Risk Factor for Stroke?

Dear Editor:

We previously suggested the possibility that aberrant carotid arteries in the area of the mouth are a new risk factor for atherosclerotic stroke.[1,2] We then speculated that stroke is associated with aberration of the internal carotid artery as follows: if the neck is bent forward, the distance between the central carotid artery and the skull base becomes shorter. To adjust to this shorter distance, a vein shortens and widens. An artery, however, cannot do so if it is atherosclerotic. Because it cannot shorten, the internal carotid artery is forced to bend. The internal carotid artery is located within the parapharyngeal space, the only nonrigid borders of which are the medial and inferior areas. For these reasons, the mouth is anatomically the most likely site for aberration of the internal carotid artery to occur. Marked aberration in patients with severe atherosclerosis causes turbulent blood flow that produces plaque and leads to brain infarctions.

After our previous reports, we performed routine examinations to detect signs of aberrant carotid arteries in aged patients with chronically bent (head-down) posture. We encountered five patients with bent posture without aberrant carotid arteries in the mouth region. The necks of those patients were chronically bent forward, and thus the distance between the central carotid artery and the skull base was shortened. However, even though the distance was shortened, we did not find any aberration inside the mouth, pharynx, and larynx even with fiberscopic examination by way of the nasal route. Finally, we determined that the common sign in these patients was aberration of the common carotid artery in the neck.

In general, the common carotid arteries are covered not only by the layers of the fascia but also by the sternocleidomastoid muscle (SCM) and the strap muscles of the neck. We realized that the carotid arteries were bent under the SCM in our patients. (Fig. 1) On ultrasonography, no difference in blood flow was seen between the two common carotid arteries; plaque was found inside both. Magnetic resonance imaging studies showed asymptomatic or symptomatic cerebral infarctions in all cases.

Advanced age with bent posture (cervical kyphosis) increases not only the incidence of aberration of the inter-

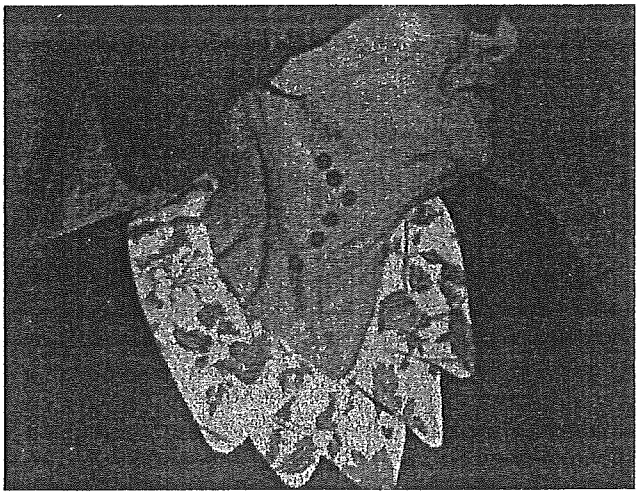

Fig. 1. The carotid arteries (red dots) were bent under the sternocleidomastoid muscle in a 74-year-old female. She had a history of stroke and atherosclerosis, with bent posture.

nal carotid artery in the mouth region but also that of aberration of the common carotid artery in the neck and may increase the risk of ischemic stroke. Ordinarily, the common carotid artery is covered by the SCM. Advanced age also results in physiologic muscle atrophy. Therefore, careful examination of the neck and mouth, simultaneously with palpation of pulsation (common carotid artery or forarm), is necessary to detect the presence of aberrant carotid arteries.

KOICHI TSUNODA
SHINICHI ISHIMOTO
National Institute of Sensory Organs
Tokyo, Japan

JO AIKAWA
MASANOBU SHINOGAMI
Nissan Tamagawa Hospital
Tokyo, Japan

RYUSUKE MURAKAMI
HIDETO SAIGUSA
Nihon Medical University
Tokyo, Japan

KENJI KONDOU
University of Tokyo
Tokyo, Japan

SEIJI BITOU
National Tokyo Medical Center
Tokyo, Japan

BIBLIOGRAPHY

1. Tsunoda K, Takanosawa M, Matsuda K. Aberrant internal carotid artery in the mouth. Lancet 1997;350:340.
2. Tsunoda K, Aikawa J, Murakami R, et al. Bent (Head-Down) posture and aberrant internal carotid artery in the mouth: a new risk factor for stroke? [Letter]. *Ann Intern Med* 2003;139:W56.

European Journal of Endocrinology (2005) 153 167–176 ISSN 0804-4643

EXPERIMENTAL STUDY

Endoplasmic reticulum stress induces *Wfs1* gene expression in pancreatic β-cells via transcriptional activation

Kohei Ueda[1], June Kawano[2], Komei Takeda[3], Toshiaki Yujiri[3], Katsuya Tanabe[3], Takatoshi Anno[3], Masaru Akiyama[3], Junichi Nozaki[4], Takeo Yoshinaga[4], Akio Koizumi[4], Koh Shinoda[2], Yoshitomo Oka[5] and Yukio Tanizawa[3]

[1]*Health Service Center, Organization for University Education, Yamaguchi University,* [2]*Division of Neuroanatomy, Department of Neuroscience, and* [3]*Division of Molecular Analysis of Human Disorders, Department of Bio-Signal Analysis, Yamaguchi University Graduate School of Medicine, 1-1-1 Minami Kogushi, Ube, Yamaguchi 755-8505, Japan,* [4]*Department of Health and Environmental Sciences, Kyoto University Graduate School of Medicine, Kyoto, Japan, and* [5]*Division of Molecular Metabolism and Diabetes, Department of Internal Medicine, Tohoku University Graduate School of Medicine, Sendai, Japan*

(Correspondence should be addressed to Y Tanizawa; Email: tanizawa@yamaguchi-u.ac.jp)

Abstract

Objective: The *WFS1* gene encodes an endoplasmic reticulum (ER) membrane-embedded protein. Homozygous *WFS1* gene mutations cause Wolfram syndrome, characterized by insulin-deficient diabetes mellitus and optic atropy. Pancreatic β-cells are selectively lost from the patient's islets. ER localization suggests that WFS1 protein has physiological functions in membrane trafficking, secretion, processing and/or regulation of ER calcium homeostasis. Disturbances or overloading of these functions induces ER stress responses, including apoptosis. We speculated that WFS1 protein might be involved in these ER stress responses.

Design and methods: Islet expression of the Wfs1 protein was analyzed immunohistochemically. Induction of Wfs1 upon ER stress was examined by Northern and Western blot analyses using three different models: human skin fibroblasts, mouse pancreatic β-cell-derived MIN6 cells, and Akita mouse-derived *Ins2* $^{96Y/Y}$ insulinoma cells. The human *WFS1* gene promoter-luciferase reporter analysis was also conducted.

Result: Islet β-cells were the major site of *Wfs1* expression. This expression was also found in δ-cells, but not in α-cells. *WFS1* expression was transcriptionally up-regulated by ER stress-inducing chemical insults. Treatment of fibroblasts and MIN6 cells with thapsigargin or tunicamycin increased *WFS1* mRNA. WFS1 protein also increased in response to thapsigargin treatment in these cells. *WFS1* gene expression was also increased in *Ins2* $^{96Y/Y}$ insulinoma cells. In these cells, ER stress was intrinsically induced by mutant insulin expression. The *WFS1* gene promoter-luciferase reporter system revealed that the human *WFS1* promoter was activated by chemically induced ER stress in MIN6 cells, and that the promoter was more active in *Ins2* $^{96Y/Y}$ cells than *Ins2* $^{wild/wild}$ cells.

Conclusion: *Wfs1* expression, which is localized to β- and δ-cells in pancreatic islets, increases in response to ER stress, suggesting a functional link between *Wfs1* and ER stress.

European Journal of Endocrinology 153 167–176

Introduction

Wolfram syndrome is a rare recessively inherited genetic disorder, which is characteristically associated with juvenile onset diabetes mellitus and progressive optic atropy (1). Sensorineural deafness, diabetes insipidus, ataxia, urinary-tract atony, peripheral neuropathy and psychiatric illness may also be present (2). We and another group succeeded in cloning the gene responsible for this disorder and designated it *WFS1* (3) or *wolframin* (4). Loss-of-function mutations in the *WFS1* gene have been linked to Wolfram syndrome. The *WFS1* gene consists of eight exons coding for a putative 890 amino acid protein with an apparent molecular mass of ~100 kDa. WFS1 protein (wolframin) is a hydrophobic protein with nine transmembrane segments and large hydrophilic regions at both termini. WFS1 protein localizes primarily to the endoplasmic reticulum (ER) in a N_{cyt}/C_{lum} membrane topology (5, 6). A recent report suggested that expression of WFS1 protein in oocytes was associated with an increase in cytosolic Ca^{2+} and induced novel cation-selective channel activities in the ER membrane (7). However, its role in cellular functions and the mechanism by which mutations of this gene cause Wolfram syndrome remain largely unknown.

DOI: 10.1530/eje.1.01945
Online version via www.eje-online.org

ER is a specialized organella involved in a wide variety of cellular functions. Calcium regulation and post-translational modification, folding and trafficking of secreted and membrane integral proteins are well-defined ER functions (8). Various physiological and pathological conditions interfere with these functions, and overloading of these functions induces ER stress. Cells respond to such stress by activating several adaptive pathways including chaperone induction, protein translation attenuation, and occasionally apoptosis, collectively called the unfolded protein response (9). Characteristically, pancreatic β-cells have highly developed ER apparently due to the heavy demands of insulin biosynthesis and secretion. Beta-cells are highly susceptible to ER stress. Several studies have shown that β-cell mass is reduced in patients with type 2 diabetes, possibly due to apoptotic death of β-cells and to reduced cell proliferation (10). ER stress may be involved in this process (11). In the Akita mouse, an animal model of MODY (maturity onset diabetes of the young), which carries a conformation-altering missense mutation (Cys96Tyr) in the insulin-2 (*Ins2*) gene (12, 13), hyperglycemia and reduced β-cell mass are accompanied by ER stress-induced β-cell death (14). Based on the ER localization of WFS1 protein, it is reasonable to speculate that WFS1 protein may play an as yet undefined role in the ER stress-induced cell death of pancreatic β-cells. In fact, we showed islet cells lacking Wfs1 to be more susceptible to ER stress-induced apoptosis (15), and, more recently, Yamaguchi *et al.* reported that treatment with ER stress inducers increased Wfs1 protein expression in isolated mouse pancreatic islets (16).

In the present study, immunohistochemical staining confirmed β-cells to be the major site of *Wfs1* expression in the mouse pancreas. Furthermore, this expression was also evident in δ-cells but not in α-cells. The *WFS1* gene was clearly expressed in response to drug-induced ER stress in both fibroblasts and pancreatic β-cell-derived MIN6 cells. Under the same conditions, the human *WFS1* promoter luciferase reporter was activated suggesting transcriptional control of *WFS1* expression. Furthermore, *Wfs1* mRNA and protein levels were increased in Akita mouse-derived *Ins2* $^{96Y/Y}$ insulinoma cells, in which the ER stress response had been triggered (17). Our results demonstrate that not only drug-induced but also intrinsic ER stress leads to *WFS1* expression in pancreatic β-cells, and this occurs, at least in part, via transcriptional activation of the *WFS1* promoter. These findings further suggest a functional link between *WFS1* and ER stress responses.

Research design and methods

Tissue preparation and immunohistochemical staining of the mouse pancreas

All experimental protocols for this study were approved by the committee on the Ethics of Animal Experimentation at Yamaguchi University School of Medicine. The anti-Wfs1 antibodies were described previously (5, 15).

Double immunofluorescent staining was performed for co-localization studies. Sections were pre-incubated, bleached (18), and stained with a mixture of anti-Wfs1n (diluted 1:200) and mouse monoclonal anti-insulin (diluted 1:100; Santa Cruz Biotechnology, Santa Cruz, CA, USA), anti-glucagon (diluted 1:200; Sigma-Aldrich, St Louis, MO, USA), or anti-somatostatin (diluted 1:25; Biomeda Corporation, Foster City, CA, USA) in 0.1 M sodium phosphate buffer containing 0.3% Triton X-100, 0.1% sodium azide, and 3% normal goat serum (PBT-NGS) for 24 h at 20 °C. Next, the sections were incubated with a mixture of two secondary antibodies in PBT-NGS for 24 h at 20 °C. The secondary antibodies used were Alexa Fluor 488 conjugated with goat anti-rabbit IgG (H + L), highly cross absorbed (Molecular Probes, Eugene, OR, USA) and diluted 1:100, and an Alexa Fluor 594 conjugated to goat anti-mouse IgG (H + L), F(ab')2 fragment (Molecular Probes), diluted 1:100. The sections were coverslipped with VECTASHIELD mounting medium (Vector Laboratories, Burlingame, CA, USA). As a control, one of the two primary antibodies, for example either anti-Wfs1n or anti-insulin, was removed to check for cross-reactivity. In these control experiments, other procedures were the same as for Wfs1/insulin double staining. No cross-reactivity was observed in these experiments (data not shown).

In the case of double immunostaining for Wfs1 and pancreatic polypeptide (PP) detection, a mixture of anti-Wfs1n (diluted 1:200) and anti-PP (diluted 1:200; Linco Research, St Charles, MO, USA) was used for the primary antibody reaction. In the secondary antibody reaction step, sections were incubated in a mixture of Alexa Fluor 488 conjugated with donkey anti-rabbit IgG (H + L; Molecular Probes) diluted 1:100 and Alexa Fluor 594 conjugated to goat anti-guinea pig IgG (H + L), highly cross absorbed (Molecular Probes) and diluted 1:100 in PBT-NGS containing 3% normal donkey serum. Other procedures for Wfs1/PP double staining were the same as for Wfs1/insulin double staining.

Cell culture and reagents

The mouse insulinoma cell line, MIN6 (19), was a gift from Dr Junichi Miyazaki, Osaka University, Japan. Insulinoma cells derived from the Akita mouse and from normal littermates, *Ins2* $^{96Y/Y}$ cells and *Ins2* $^{WT/WT}$ cells respectively, were described previously (17). These cells were maintained in Dulbecco's modified Eagle's medium (DMEM) (Sigma) supplemented with 15% fetal calf serum in an atmosphere of 5% CO_2 at 37 °C. The genotype for the insulin-2 gene was confirmed by restriction fragment length polymorphism (RFLP), as previously described (12, 13). Human skin fibroblasts

(CCD-1059SK) were obtained from ATCC (Manassas, VA, USA). Thapsigargin, ionomycin, A23187, cyclopiazonic acid, 4-chloro-*m*-cresol, tunicamycin and brefeldin A were purchased from Sigma.

Northern blot analysis

Total RNA isolated using an ISOGEN kit (NIPPON GENE, Tokyo, Japan) was electrophoresed in 1% agarose formaldehyde gel and transferred to nylon filters (Hybond-N plus, Amersham Pharmacia Biotech). The filters were prehybridized and hybridized in a buffer containing 50% deionized formamide, 5 × sodium chloride-sodium phosphate-EDTA buffer (750 mmol/l NaCl, 43.25 mmol/l NaH_2PO_4, 6.25 mmol/l EDTA), 2 × Denhardt's solution (0.04% bovine serum albumin, 0.04% Ficoll, 0.04% polyvinylpyrrolidone), and 0.1% soduim dodecyl sulfate at 42 °C. The hybridization buffer contained a radio-labeled 3.0 kb fragment of mouse *Wfs1* cDNA (GeneBank Accession No. BC046988). After a stringent wash with 0.2 × sodium chloride-sodium citrate buffer (3.3 mmol/l Na-citrate, 3.3 mmol/l NaCl) and 0.1% SDS at 50 °C, autoradiographs were digitally scanned and quantified using FULA2000 (Fuji Film, Tokyo, Japan). The blots were stripped and re-proved with a 1122 bp fragment encompassing the entire coding region of the mouse glyceraldehyde-3-phosphate dehydrogenase (GAPDH) cDNA. The cDNA probes were labeled with a random primer DNA labeling kit (Ready-To-Go DNA Labeling Beads, Amersham Pharmacia Biotech) using α-[^{32}P]deoxy-CTP (Amersham Pharmacia Biotech).

Immunoblotting analysis

Cells were lysed in 20 mmol/l Tris–HCl (pH 7.6), 0.5% Nonidet P-40, 250 mmol/l sodium chloride, 3 mmol/l EDTA, 3 mmol/l EGTA, 1 mmol/l phenylmethylsulfonyl fluoride, 2 mmol/l sodium orthovanadate, 20 μg/ml aprotinin, 1 mmol/l dithiothreitol and 5 μg/ml leupeptin. Proteins in cell lysates were separated in 10% SDS-PAGE gel and then electrophoretically transferred onto a nitrocellulose membrane. All membranes were stained with Ponceau S to confirm equal protein loading. The membrane was blocked with 5% milk in TBS-T (50 mmol/l Tris–HCl, 300 mmol/l NaCl, pH 7.6, 0.1% Tween 20) for 1 h. SDS-PAGE and immunoblotting were carried out as described previously (20). Anti-Bip (GRP74), anti-Chop, anti-phosphorylated eIF2-α, and anti-poly(ADP-ribose) polymerase (PARP) antibodies were purchased from Santa Cruz Biotechnology. Detection was performed using the ECL system (Amersham Pharmacia Biotech).

Luciferase assay

To construct the *WFS1* promoter-luciferase reporter gene, the promoter region of the human *WFS1* gene (−3000 to +20, Genbank Accession No. AC004689) was PCR-amplified from human genomic DNA. The fragment was inserted upstream from the luciferase cDNA in a pGL3-Basic vector (Promega, Madison, WI, USA). A plasmid, pCMVβ (Clontech, Palo Alto, CA, USA), containing the cytomegalovirus (CMV) promoter-driven β-galactosidase gene was used as an internal control for the normalization of transfection efficiency. One day before transfection, MIN6 cells or *Ins2*$^{96Y/Y}$ cells were plated at 1×10^5/well into 6-well tissue culture plates. The reporter plasmid (0.5 μg) and the pCMVβ (0.5 μg) were co-transfected into MIN6 cells or *Ins2*$^{96Y/Y}$ cells in 6-well tissue culture plates using 10 μl LipofectAMINE 2000 (Invitrogen) in serum-free Opti-MEM medium (Invitrogen). Twenty-four hours after transfection, the medium was changed to DMEM containing 15% fetal calf serum and 20 mmol/l glucose, and cultured for a further 24 h. After this 24-h incubation, MIN6 cells were treated with thapsigargin or tunicamycin for an additional 6 h. Cell extracts were prepared, and luciferase and β-galactosidase activities were determined using a β-galactosidase enzyme assay system according to the manufacturer's protocol (Promega).

Results

Wfs1 *expression in the mouse pancreatic islet*

Using immunohistochemistry, it was demonstrated that mouse Wfs1 protein was widely expressed in pancreatic islets except in some peripheral areas, while no signals for Wfs1 protein were detected in exocrine acinar cells (Figs 1 and 2 and data not shown). Using double-immunofluorescent staining, the majority of Wfs1-immunoreactive cells were found to coincide with insulin-producing β-cells. Some minor part of the Wfs1 immunoreactivity was, however, localized to non-β-cells seen in the islet periphery (Fig. 1A–F). Such Wfs1-immunoreactive non-β-cells were found to correspond to somatostatin-producing δ-cells (Fig. 1G–L). There was little difference in Wfs1-immunoreactive intensity between the two endocrine cell types (Fig. 1). Wfs1-immunoreactivity was not evident in glucagon-producing α-cells or in pancreatic polypeptide cells (PP-cells; Fig. 2).

ER stress induces WFS1 *expression in fibroblasts*

ER stress induces cellular responses, collectively termed the unfolded protein response, affecting diverse areas of cellular function such as gene expression, metabolism, cell signaling and apoptosis. Certain reagents are known to disturb ER calcium homeostasis or to inhibit post-translational processing or sorting, and thereby to cause ER stress (9). Chemical insults inducing ER stress, the calcium ionophor A23187 and ionomycin,

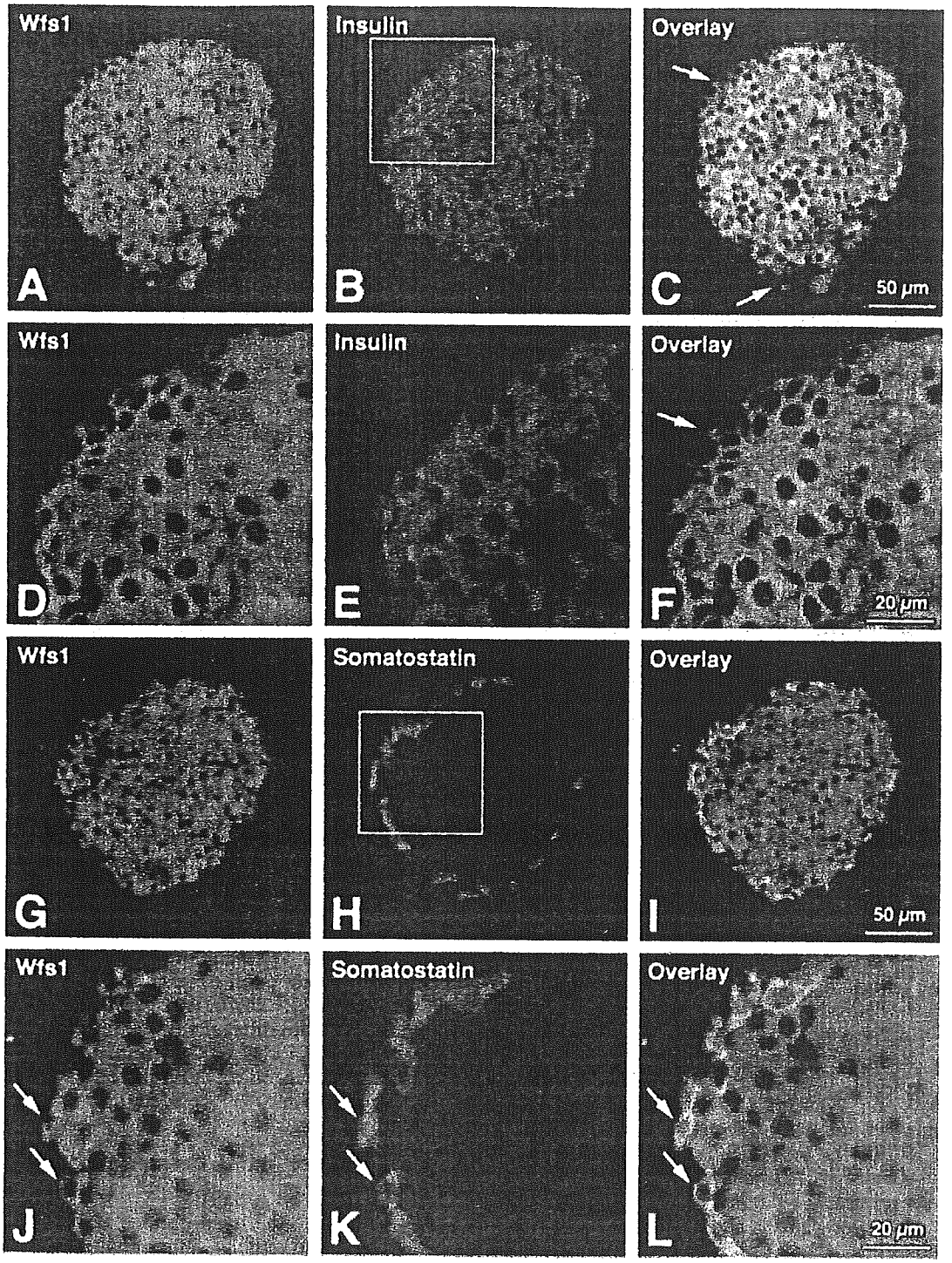

Figure 1 Mouse Wfs1 protein, insulin and somatostatin expression in mouse pancreatic islets. Double immunostaining for mouse Wfs1 (Wfs1: A, D, G, J; Alexa Fluor 488 label; green) and pancreatic hormones (insulin: B, E; somatostatin: H, K; Alexa Fluor 594 label; red) was performed. Panels C, F, I and L are overlaid images. All fluorescent photomicrographs were taken with a confocal microscope LSM 510 (Carl Zeiss Jena GmbH, Jena, Germany). The approximate positions of E and K are indicated by the rectangular frames in B and H respectively. Small solid arrows in C and F indicate non-β endocrine cells immunoreactive for Wfs1. Small solid arrows in J, K and L show somatostatin-producing δ-cells strongly immunoreactive for Wfs1. Note that insulin-producing β-cells and somatostatin-producing δ-cells display Wfs1 immunoreactivity. Scale bars = 50 μm in C and I for A, B, and for G, H; 20 μm in F and L for D, E, and for J, K.

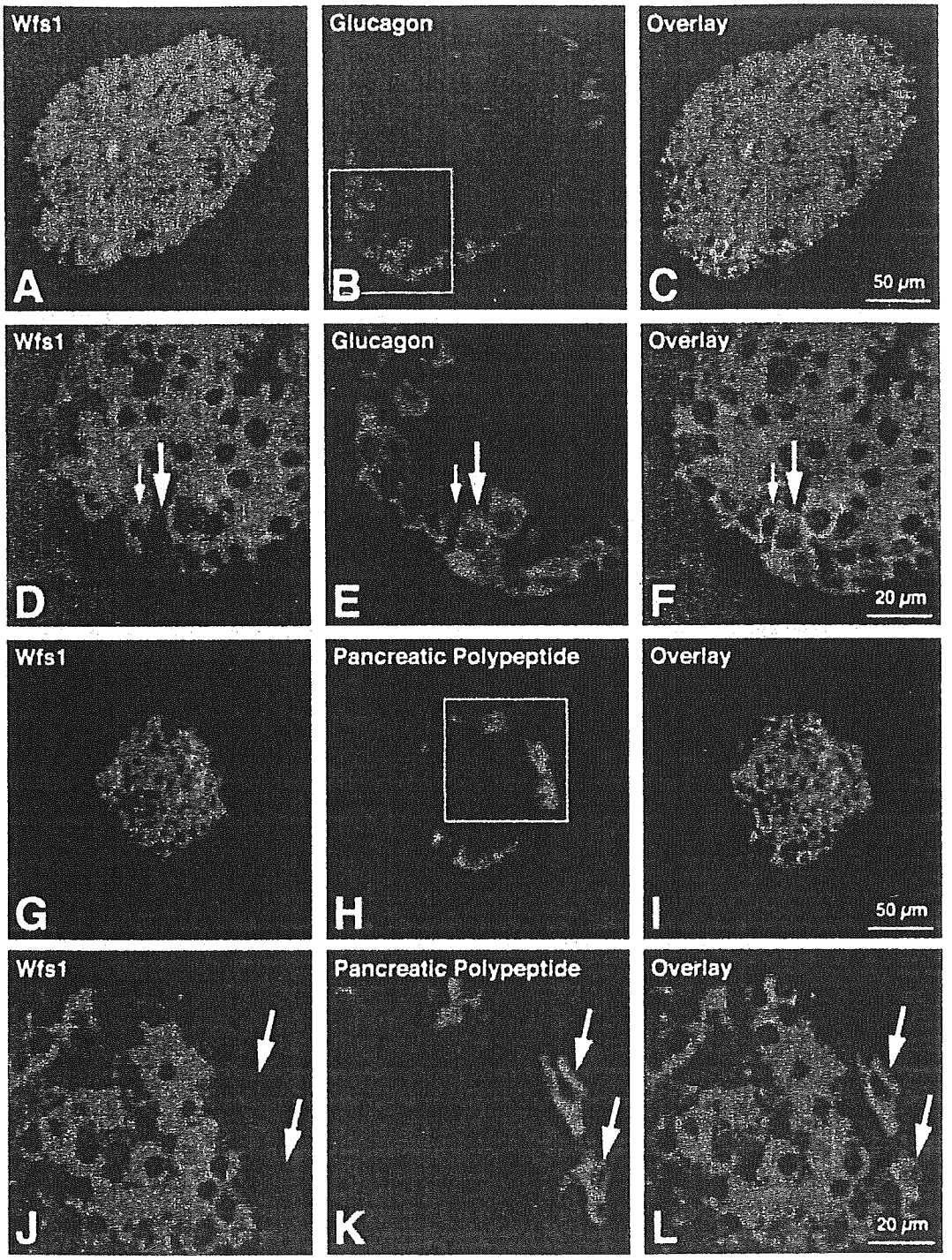

Figure 2 Mouse Wfs1 protein, glucagon and pancreatic polypeptide expression in mouse pancreatic islets. Double immunostaining for mouse Wfs1 (Wfs1: A, D, G, J; Alexa Fluor 488 label; green) and pancreatic hormones (glucagon: B, E; pancreatic polypeptide: H, K; Alexa Fluor 594 label; red) was performed. Panels C, F, I and L are overlaid images. All fluorescent photomicrographs were taken with a confocal microscope LSM 510 (Carl Zeiss Jena GmbH). The approximate positions of E and K are indicated by the rectangular frames in B and H respectively. Large and small solid arrows in D, E and F indicate glucagon-producing α-cells negative for Wfs1 immunoreactivity and non-α endocrine cells positive for Wfs1 immunoreactivity respectively. Large solid arrows in J, K and L show pancreatic polypeptide cells (PP-cells) negative for Wfs1 immunoreactivity. Scale bars = 50 μm in C and I for A, B, and for G, H; 20 μm in F and L for D, E, and for J, K.

the ER Ca^{2+}-ATPase inhibitors (21) thapsigargin and cyclopiazonic acid, the ryanodine receptor activator 4-chloro-*m*-cresol, and the protein *N*-glycosylation inhibitor tunicamycin all induced WFS1 protein as shown in Fig. 3. Only brefeldin A had no effect. Ionomycin only weakly induced WFS1 protein. The differing effects of these chemicals, which have different mechanisms of action, may provide insights into the functions of Wfs1. The lack of WFS1 induction with brefeldin A, a Golgi apparatus disruptor, may be related to its instability in solution (22). Although we did not perform Northern blot analysis for each of these reagents, A23187 induced *WFS1* mRNA in fibroblasts (data not shown).

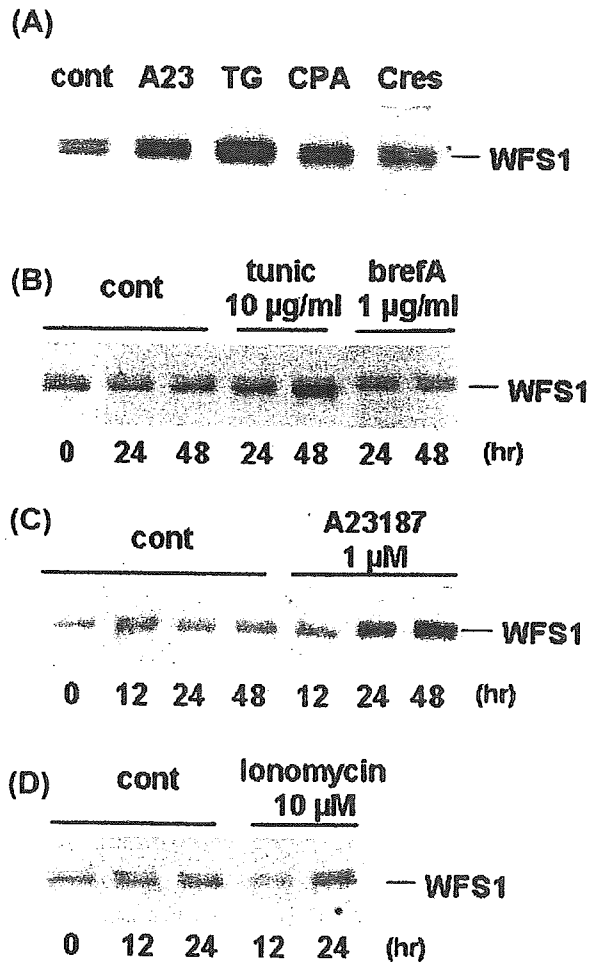

Figure 3 ER stress induces WFS1 protein in fibroblasts. Primary skin fibroblasts were cultured in the presence of (A) A23187 (A23, 1 μmol/l), thapsigargin (TG, 1 μmol/l), cyclopiazonic acid (CPA, 10 μmol/l) and 4-chloro-*m*-cresol (cres, 50 μmol/l) for 48 h. (B–D) Cells were treated for the indicated time periods with (B) tunicamycin (tunic), brefeldin A (brefA), (C) A23187, and (D) ionomycin. cont indicates control. Control samples included a vehicle (DMSO), also administered with all of the drugs. Cells were harvested after the incubation periods, and total cell lysates containing 20 μg protein were subjected to Western blot analysis using anti-WFS1c antibody.

Effects of thapsigargin and tunicamycin on Wfs1 expression in MIN6 cells

We next examined the effects of thapsigargin and tunicamycin on the expression of *Wfs1* mRNA in MIN6 cells. Thapsigargin and tunicamycin treatments are known to induce ER stress, and Chop/GADD153 is a transcription factor that plays a role in ER stress-induced apoptotic cell death (23, 24). Phosphorylation of the α-subunit of translation initiation factor-2 (eIF2-α) attenuates protein translation upon ER stress. Although the ER chaperone Bip/GRP78 expression did not change in MIN6 cells (Fig. 4B) probably due to its strong basal expression, thapsigargin and tunicamycin clearly generated ER stress as demonstrated by Chop induction and eIF2-α phosphorylation (Fig. 4A, B). Under these conditions, ER stress-induced caspase-3 activation, an event at the initiation of apoptosis (25), was evidenced by the cleavage of PARP (Fig. 4C). PARP is one of the substrates cleaved by caspase-3. Upon thapsigargin or tunicamycin treatment, the 113 kDa band decreased, and instead, the proteolytic PARP fragment (89 kDa) appeared (Fig. 4C). In association with ER stress induction and caspase-3 activation, *Wfs1* mRNA expression increased (Fig. 4A,D). With thapsigargin, *Wfs1* mRNA started to increase after 6 h and was maximal after 12 h. With tunicamycin, *Wfs1* mRNA induction peaked at 6 h, and then declined. Wfs1 protein was also increased by thapsigargin treatment (Fig. 4B). In contrast, tunicamycin, despite the mRNA induction, did not increase the Wfs1 protein, but decreased it after 24 h (Fig. 4B). This is probably due to the instability of unglycosylated Wfs1 protein (6, 16).

Thapsigargin and tunicamycin enhance human WFS1 promoter activity in MIN6 cells

To determine the mechanism of *WFS1* expression, we examined the effects of thapsigargin and tunicamycin on human *WFS1* gene promoter activity by employing transient transfection assays in MIN6 cells. We used a *WFS1* promoter-luciferase construct that contained a 3 kb DNA sequence upstream from the human *WFS1* gene transcription initiation site. The human *WFS1* gene promoter was active in MIN6 cells. Introduction of the *WFS1* promoter-reporter plasmid produced a 20-fold increase in luciferase activity as compared with the promoterless pGL3-Basic vector. Treatment of the cells with thapsigargin or tunicamycin resulted in further 1.3- and 1.5-fold increases in luciferase activity respectively (Fig. 5). We conducted these experiments again using a 1 kb (−1000 to +20) *WFS1* promoter-luciferase reporter gene. The results were essentially the same but the promoter activity was weaker than with the 3 kb construct (data not shown).

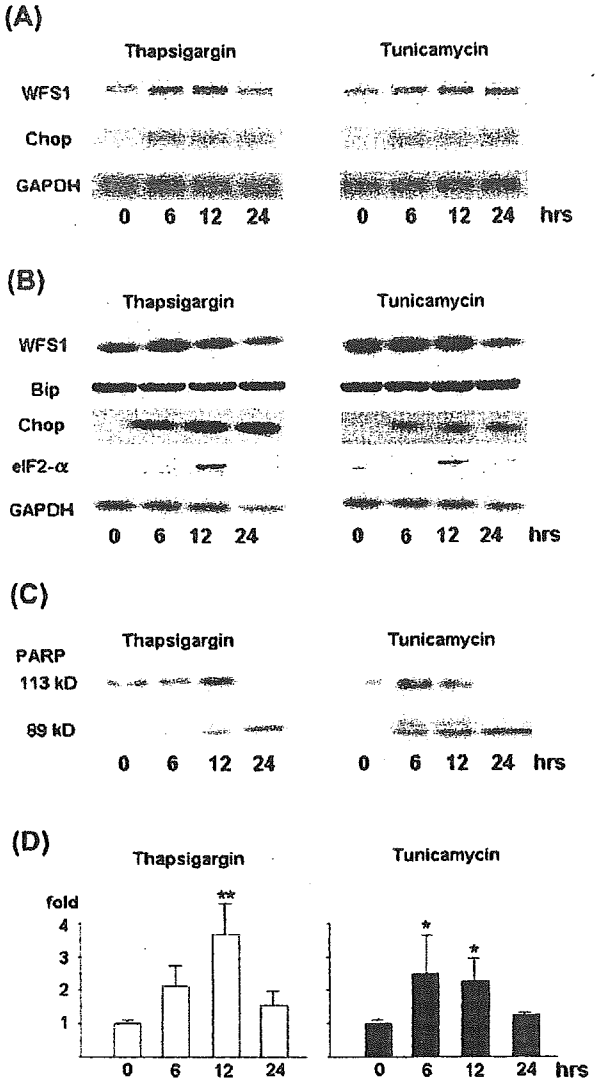

Figure 4 Thapsigargin and tunicamycin increase *Wfs1* mRNA expression in MIN6 cells in association with ER stress and apoptosis induction. MIN6 cells were placed in culture dishes and serum-starved in serum-free DMEM for 12 h, and then treated with thapsigargin (1 μmol/l) or tunicamycin (10 μg/ml) for 6, 12 or 24 h. Dimethyl sulfoxide (DMSO) was used to dissolve thapsigargin and tunicamycin, and the same concentration of DMSO (final, 0.05%) was employed in all experiments, including controls. After incubation, cells were washed once with ice-cold phosphate-buffered saline, and harvested. (A) Ten micrograms RNA were subjected to Northern blot analysis. (B) Total cell lysates containing equal amounts of protein (50 μg) were separated on 10% SDS-PAGE and analyzed by immunoblotting using anti-Wfs1n, anti-Bip (GRP74), anti-Chop or anti-phosphorylated eIF2-α, (C) Total cell lysates containing equal amounts of protein (50 μg) were separated on 10% SDS-PAGE and analyzed by immunoblotting using the anti-PARP antibody. Activated caspase-3 cleaves the 113 kDa PARP, resulting in the appearance of the 89 kDa fragment. (D) Quantification of the *Wfs1* mRNA from the results obtained in (A), shown as means±S.E. ($n = 4$). Statistical analysis, conducted using analysis of variance, indicated that the thapsigargin and tunicamycin treatments significantly increased *Wfs1* mRNA expression at 12 h and at 6 h and 12 h respectively (*$P < 0.05$, **$P < 0.001$).

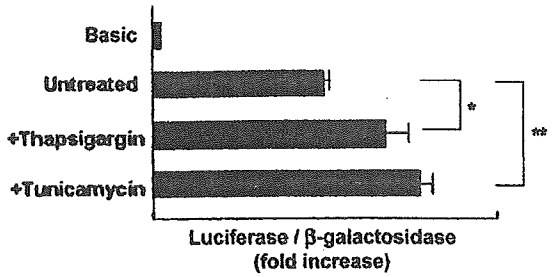

Figure 5 ER stress enhances *WFS1* promoter activity in MIN6 cells. MIN6 cells were transfected with a luciferase reporter plasmid containing a 3.0 kb human *WFS1* gene 5' flanking promoter region (from −3000 to +20) and were exposed to thapsigargin (1 μmol/l) or tunicamycin (10 μg/ml) for 6 h. Beta-galactosidase activity from the co-transfected expression vector pCMVβ was used to calibrate for transfection efficiency. Basic represents luciferase activity from pGL3-Basic (promoterless) vector-transfected cells. Results are expressed as the fold increase as compared with basic (means±S.E. of four independent experiments, each performed in triplicate). *P* values for comparison of results with versus without drug treatments are 0.034 (thapsigargin, *) and 0.005 (tunicamycin, **) (analysis of variance).

Wfs1 *expression is transcriptionally upregulated in β-cells with intrinsic ER stress*

In the Akita mouse, the C96Y mutation of the *ins2* gene disturbs intramolecular disulfide bond formation, resulting in progressive β-cell loss (12). ER stress and subsequent apoptosis are at least partially responsible for this progressive β-cell loss (14). To further examine the association between increased *Wfs1* expression and ER stress, we used mouse insulinoma cells derived from an Akita mouse homozygous for the *ins2* gene C96Y mutation (*Ins2* $^{96Y/Y}$ cell) as a model. *Ins2* $^{WT/WT}$ cells derived from normal littermates served as controls. Doubling of the ER chaperone Bip/GRP78 in *Ins2* $^{96Y/Y}$ cells indicated persistent ER stress in these cells (Fig. 6A). In Ins2$^{96Y/Y}$ cells, Wfs1 protein increased sixfold as compared with that in *Ins2* $^{WT/WT}$ cells (Fig. 6B). *Wfs1* mRNA expression was also increased twofold (data not shown). We next examined *WFS1* promoter activity in these cells. Introduction of the *WFS1* promoter-reporter plasmid into *Ins2* $^{96Y/Y}$ cells approximately doubled luciferase activity as compared with that in wild type *Ins2* $^{WT/WT}$ cells (Fig. 7). Luciferase activity after transfection of the SV40 promoter-reporter plasmid did not differ between *Ins2* $^{96Y/Y}$ and *Ins2* $^{WT/WT}$ cells.

Discussion

Herein, we have documented the localization of Wfs1 expression in the mouse pancreatic islet. Insulin-producing β-cells are the major site of Wfs1 expression, as shown in Ishihara *et al.* (15). Wfs1 expression is also evident in somatostatin-producing δ-cells, but is absent from glucagon producing α-cells and PP-cells. No *Wfs1* expression is observed in pancreatic exocrine acinar

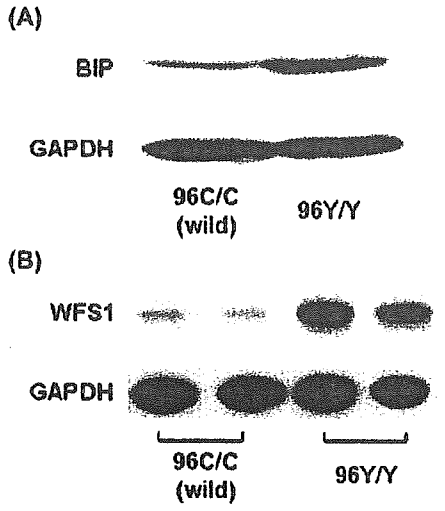

Figure 6 *WFS1* expression is increased in Akita mouse-derived *Ins2*$^{96Y/Y}$ cells. Cell extracts of *Ins2*$^{96Y/Y}$ cells containing equal amounts of protein (50 μg) were separated on 10% SDS-PAGE and analyzed by immunoblotting using (A) anti-Bip, and (B) anti-WFS1n and anti-GAPDH antibodies. Insulinoma cells derived from wild type littermates (wild) were used as the control. In (B), cell extracts were prepared on two separate occasions from cells derived from the same mutant mouse.

cells. A histopathological study of pancreatic islets from Wolfram syndrome patients showed selective loss of insulin-producing β-cells and an apparent preservation of glucagon-producing α-, somatostatin-producing δ-, and PP-cells (26, 27). The histochemical evidence of Wfs1 protein localization in insulin-producing β-cells might provide a histological background explaining the insulin deficiency caused by *WFS1* mutations in Wolfram syndrome patients and suggests that WFS1 protein is necessary for β-cell (28, 29), but not δ-cell survival.

We have also presented evidence herein that ER stress induces *Wfs1* gene expression. Treatment of fibroblasts with A23187, ionomycin, thapsigargin, cyclopiazonic acid, 4-chloro-*m*-cresol or tunicamycin increased *Wfs1* protein levels. Chemical insults by these reagents are known to induce ER stress via disruption of Ca^{2+} homeostasis or inhibition of N-linked glycosylation. Thapsigargin and tunicamycin treatments also induced *Wfs1* mRNA expression in a mouse β-cell line, MIN6 cells. In accordance with the mRNA change, thapsigargin increased Wfs1 protein expression. However, the Wfs1 protein level in MIN6 cells did not change with tunicamycin. This is probably due to Wfs1 being an N-glycosylated protein, and inhibition of glycosylation by tunicamycin decreases its stability (6, 16). Increased *Wfs1* expression in association with ER stress was further demonstrated in another β-cell model with ER stress: *Ins2*$^{96Y/Y}$ cells derived from the Akita mouse. The Akita mouse spontaneously develops early-onset non-obese diabetes with a reduced β-cell mass, which is caused by a conformation-altering missense mutation (Cys96Tyr) in the insulin-2 gene (12, 13). Intramolecular disulfide-bond formation is disrupted in the mutant insulin molecule. It was reported that this misfolded mutant insulin expression constitutively induced ER stress in Akita mouse β-cells (14). We have indeed confirmed increased Bip protein expression in *Ins2*$^{96Y/Y}$ cells as compared with wild type *Ins*$^{WT/WT}$ cells derived from normal littermates. In *Ins2*$^{96Y/Y}$ cells, *Wfs1* mRNA (data not shown) and protein levels (Fig. 6) were both increased. The increased *Wfs1* mRNA (twofold, data not shown) was consistent with the increased *Wfs1* promoter activity (Fig. 7). Our results provide further evidence, i.e. a detailed analysis, that *Wfs1* expression increases in association with ER stress, especially in the pancreatic β-cells selectively lost in patients with Wolfram syndrome. It is noteworthy that the increase in Wfs1 protein was marked (sixfold) as compared with the modest increase in Bip expression (twofold) in *Ins2*$^{96Y/Y}$ cells. Mechanisms other than ER stress might have further increased Wfs1 protein expression in this cell line.

The increase in *Wfs1* expression is attributable, at least in part, to enhanced *Wfs1* transcription, because both ER stress-inducing chemical insults (MIN6 cells) and intrinsic ER stress (*Ins2*$^{96Y/Y}$cells) stimulated *WFS1* promoter activity as demonstrated by a transient transfection assay using a human *WFS1* promoter-luciferase reporter construct. A cis-acting ER stress responsive element (ERSE) has been identified in the proximal promoter regions of chaperone-encoding genes. This element consists of a consensus sequence of

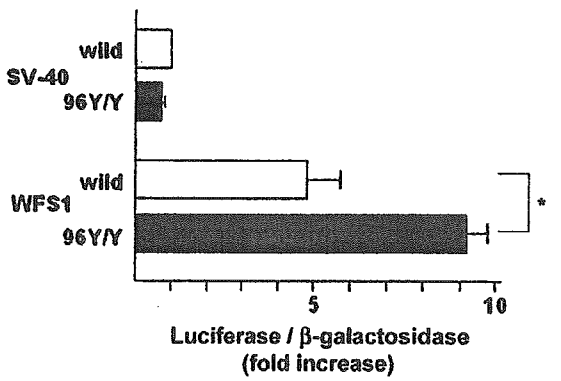

Figure 7 *WFS1* promoter activity is enhanced in *Ins2*$^{96Y/Y}$ cells. *Ins2*$^{96Y/Y}$ cells or wild type (wild) control cells were transfected with a luciferase reporter plasmid containing the 3.0 kb human *WFS1* gene 5' flanking promoter region (from −3000 to +20), or a control plasmid containing the SV40 promoter-luciferase reporter. The expression vector pCMVβ was co-transfected, and β-galactosidase activity was used to calibrate for transfection efficiency. Results are expressed as fold-increases relative to luciferase/β-galactosidase activities in *Ins2*$^{96Y/Y}$cells as compared with control *Ins2*$^{WT/WT}$ cells in four independent experiments (means±S.E.), each performed in triplicate. *WFS1* promoter activity was significantly increased in *Ins2*$^{96Y/Y}$ cells as compared with control *Ins2*$^{WT/WT}$ cells (*$P = 0.014$, Student's *t*-tests).